Biophysical Society

Background Suppression in Imaging Gold Nanorods through Detection of Anti-Stokes Emission

Aquiles Carattino,[1] Veer I. P. Keizer,[2] Marcel J. M. Schaaf,[2] and Michel Orrit[1,*]

[1]Leiden Institute of Physics, Leiden, the Netherlands; and [2]Institute of Biology and Molecular Cell Biology, University of Leiden, Leiden, the Netherlands

ABSTRACT   Metallic nanoparticles have opened the possibility of imaging, tracking, and manipulating biological samples without time limitations. Their low photoluminescence quantum yield, however, makes them hard to detect under high background conditions. In this study we show that it is possible to image gold nanorods by detecting their anti-Stokes emission under resonant excitation. We show that even in the membrane of a cell containing the fluorescent dye Atto 647N, the signal/background of the anti-Stokes emission can be >10, while it is impossible to image the particles with the Stokes emission. The main advantage of this technique is that it does not require any major change in existing fluorescence imaging setups, only the addition of an appropriate short-pass filter in the detection path.

INTRODUCTION

High-resolution microscopy has become an indispensable tool for studying biological samples both in vitro and in vivo (1). Fluorescent organic dyes are commonly employed to such ends because of their reduced size and high quantum yield (2). Fluorophores, however, have an inherent constraint in the possible observation time, because molecules eventually bleach under intense illumination (3). Even the most photostable dyes cannot be imaged at saturation for longer than few tens of seconds. Gold nanoparticles on the other hand are almost indefinitely stable (4) and open up many original applications including photothermal therapy (5) and imaging (6).

As gold nanoparticles do not blink nor bleach (7,8), they are ideal candidates for labeling (9), tracking (10), and manipulating (11) biological samples over extended periods of time. Moreover it has been shown that with the proper size and coating, they do not interfere with cells' functioning (12), allowing not only in vitro but also in vivo studies. Compared to organic dyes, gold nanoparticles are much larger and their emission quantum yield is much smaller, in the order of 10^{-6} (13). This minute value is compensated by an absorption cross section several orders of magnitude larger than that of molecules (14), therefore

the brightness of gold nanoparticles is comparable to that of fluorescent molecules under the same illumination intensity.

Because the absorption cross section of the particles scales as their volume, detecting smaller particles in the presence of background requires a specific approach. Several techniques have been proposed, including two-photon excitation (6), photothermal heterodyne detection (15), and interferometric detection (16). Each of these methods is useful, but their operation requires dedicated setups and a high level of expertise. A method that allows us to image gold nanoparticles with a high background rejection and that is readily implementable in current confocal and wide-field microscopes would provide great benefits.

Gold nanoparticles exhibit a collective oscillation of conduction electrons called surface plasmon resonance (17). This resonance strongly depends on the shape of the particles (18,19). Spheres with radius roughly between 5 and 80 nm will have a resonance between 520 and 560 nm; more elongated particles such as nanorods or bipyramids (20) exhibit red-shifted longitudinal resonances that reach wavelengths of 800 nm or longer (21). It is important to note that tuning the shape of the particles can be easily achieved by synthesis and that relatively narrow size distributions can be obtained (22).

The plasmon is responsible for enhanced absorption and scattering cross sections (23) of particles for specific

CrossMark

wavelengths but it is also responsible for enhanced photoluminescence emission in the spectral region of the plasmon resonance. In this work, luminescence is referred to all the emission arising from a nanoparticle at wavelengths that are different from the excitation wavelength. Because of the absence of a gap in the excited states' spectrum of gold nanoparticles, their photoluminescence excitation spectra overlaps their emission spectrum (13), a very different situation from the Stokes-shifted emission of fluorescent molecules and semiconductor nanocrystals. Upon excitation of gold nanoparticles at their plasmon resonance maximum, most of the emission will be concentrated in a narrow spectral region around the excitation. A portion of the luminescence emission will therefore have the same wavelength than the excitation, making it indistinguishable from elastic scattering. But this region of the spectrum will be blocked by the filters that, in fluorescence detection experiments, prevent direct excitation light from reaching the detectors.

It is also possible to excite the particles off-resonance with a shorter wavelength laser (for instance through interband transitions with 532 nm) and the emission will be mostly concentrated around the longitudinal plasmon resonance of nanorods at longer wavelengths. This is the closest situation to the behavior of a fluorophore, in which the Stokes-shifted emission can be easily detected by introducing a long-pass filter. The drawback, however, is that the cross section of particles is much smaller at this wavelength and can only be compensated by increasing the excitation power.

Fig. 1 shows typical spectra of a gold nanorod under different excitation wavelengths. The green curve is the one-photon-excited luminescence spectrum around the longitudinal plasmon resonance, observed while irradiating with 532 nm laser; the full spectrum of the longitudinal plasmon is clea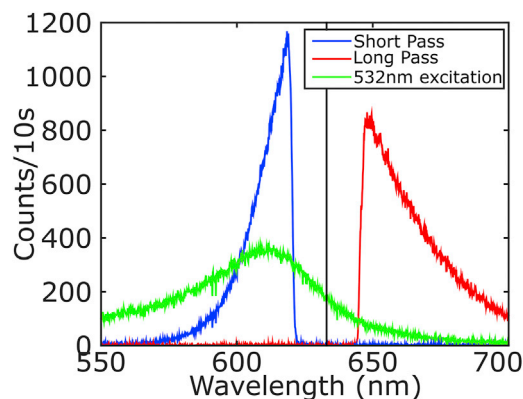rly observable with its resonance at 620 nm. The particle can also be excited at or close to its resonance, where its absorption cross section is maximum.

Fig. 1 shows the emission spectra upon excitation at 633 nm, depicted as the vertical black line. The red curve is the Stokes-shifted emission; the spectral shape of this emission overlaps with the one observed exciting at 532 nm. Exciting in resonance is more efficient and therefore the emission is much brighter. The blue curve in Fig. 1 displays the anti-Stokes emission at shorter wavelengths. In this case the spectral shape does not resemble that of the plasmon resonance. The exponential-like decay of the anti-Stokes spectrum can be modeled with Boltzmann statistics (24) of the bath (phonons and electrons) energy levels that are present in gold nanoparticles at room temperature. In both cases it is clear from the shape of spectra that the filters block an important part of the emission close to the plasmon maximum.

This work focuses in the exploitation of the anti-Stokes luminescence (25) for imaging of gold nanorods in biologically relevant conditions. This scheme benefits from the enhanced absorption cross section of the particles, their high photostability, and fairly narrow emission spectra. When exciting in resonance with the plasmon, a short-pass filter can be introduced allowing the observation of only the anti-Stokes emission. This procedure highly reduces the background arising from self-fluorescence and Raman-scattering from cells, most of it being Stokes-shifted. Reducing the background therefore opens the possibility of imaging and tracking smaller particles or using lower excitation powers.

The anti-Stokes emission mechanism (24) is depicted in Fig. 2 and can be described as follows: an absorbed photon
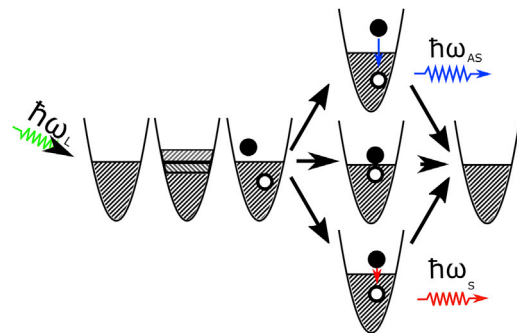

FIGURE 2 Schematic of the anti-Stokes luminescence arising from a single gold nanorod. After excitation with a photon, a collective oscillation of electrons is generated. Once the coherence is lost, the state can be described as an electron-hole pair. Three scenarios are possible: electron and hole may recombine radiatively after one of more interactions with the thermal baths of lattice phonons and charge carrier thermal excitations: 1) if the energy difference between electron and hole states is lower than the initial one after excitation we obtain Stokes emission upon a radiative recombination; 2) if electron and hole transiently increase their energy difference at the bath's expense before recombining radiatively, we observe anti-Stokes emission; and 3) if electron and hole recombine nonradiatively, their energy difference is transferred to the baths and no photon is emitted. (The latter process is the most probable one.) To see this figure in color, go online.

FIGURE 1 Luminescence spectra of a single gold nanorod. (*Green curve*) Emission upon excitation with a 532 nm laser. (*Red curve*) Stokes emission upon excitation with a resonant 633 nm HeNe laser. (*Blue curve*) Anti-Stokes emission under the same 633 nm excitation. To see this figure in color, go online.

generates a collective oscillation of the conduction electrons. After a fast loss of the coherence (26), the state of the particle can be described as an electron-hole pair. After one or more interactions with the thermal baths, i.e., with phonons of the gold lattice (27) or thermally excited charge carriers (28), the hole and/or the electron can receive energy. This energy can transiently increase the energy difference between electron and hole; if then they recombine radiatively, the emitted photon will have a shorter wavelength (higher energy) than the incoming photon (29). The same mechanism accounts for the Stokes-shifted emission, the only difference being that the electron-hole pair has lost energy to the baths before recombining radiatively. Finally, electron and hole can recombine nonradiatively, transferring their whole energy to the lattice.

The probability of a radiative recombination of electrons and holes is low, as can be experimentally determined by the very low emission quantum yield of the photoluminescence (13,20,26). Anti-Stokes emission stems from electron-hole recombination events after the electron-hole pair has transiently gained energy from the lattice, i.e., before it thermalizes. Even if the anti-Stokes scenario is unlikely, it is frequent enough as to observe an intensity in the range of 10^3 counts per second on an avalanche photodiode with excitation powers at ~16 kW/cm^2. Such relatively high detection rates require enhancement of the emission probability through the proximity of the plasmon resonance (30).

The main advantage of the approach presented in this work is the simplicity of its implementation. With any confocal or wide-field setup enabling resonant excitation of gold nanoparticles, one can exploit the anti-Stokes photoluminescence by inserting a proper short-pass filter in the detection path. As we will see below, single gold nanoparticles can be detected even in higher background conditions such as a stained cell, or a highly self-fluorescent sample.

MATERIALS AND METHODS

Images of gold nanorods were recorded by sample scanning, employing a XYZ piezo stage (PI Nano Cube; Physik Instrumente, Karlsruhe, Germany) in a home-built confocal microscope, sketched in Fig. S1 *a* in the Supporting Material. The objective employed was an oil-immersion Olympus 60× NA 1.4 (Melville, NY) that allowed a high efficiency in both exciting the particles and collecting their emission. The luminescence arising from the particles was filtered and detected by either an avalanche photodiode or a liquid-nitrogen-cooled CCD-spectrometer (Acton 500i; Acton Research, Acton, MA). An example of an image can be seen in Fig. S1 *b*. To detect the anti-Stokes luminescence, a 633 nm short-pass filter (Semrock, Rochester, NY) was added to the detection path together with a 633 nm notch filter. Both filters were needed simultaneously because neither of them was able to entirely block the excitation light from the detectors. The Stokes luminescence was collected replacing the short-pass filter with a 633 nm long-pass (Semrock).

Gold nanorods were synthesized by following the standard seeded-growth method (22). The average size of the nanorods was 50 × 23 nm and their SPR was located at ~650 nm in water. Fig. S2 shows the extinction spectrum of a suspension of the nanoparticles after synthesis and Fig. S4 shows a transmission electron microscopy image of the rods.

Two different laser wavelengths were employed. A CW 532 nm laser (Changchun New Industries, Changchun, China) was used to excite the transverse plasmon and the full longitudinal plasmon spectrum was collected. Single nanorods exhibit a narrow Lorentzian-shaped luminescence spectrum as displayed in Fig. S1 *c*. A second CW laser (Thorlabs HeNe; Thorlabs, Newton, NJ) with a wavelength of 633 nm allowed us to excite the particles in resonance and collect either the Stokes or the anti-Stokes emission depending on the analysis filters. Both lasers were focused to a diffraction-limited spot through the high NA objective.

Fig. 3 shows a scatter plot of the Stokes and anti-Stokes emission intensities of 75 gold nanorods against their plasmon peak position. The anti-Stokes emission was calculated by integrating the recorded spectra at wavelengths shorter than the excitation laser, while the opposite was done for the Stokes. This can also be directly measured by recording the emission intensity after a short-pass or long-pass filter. The large dispersion of the points observed can be attributed to the distribution of sizes of the rods inherent to the synthesis method (31) (bigger particles will have a bigger cross section) and probably to different photoluminescence quantum yields for different individual particles. Because the particles were first deposited on glass directly and because they were excited with circularly polarized light, their orientation should not influence their photoluminescence intensity.

It is possible to observe that the maximum emission intensity for the anti-Stokes appears for those particles with their plasmon slightly blue shifted from the laser wavelength, while the opposite is observed for the Stokes emission. This means that there is a trade-off between the excitation efficiency and the collection efficiency: exciting in perfect resonance is more efficient, but the filters will eliminate most of the luminescence. Therefore exciting slightly to the blue (*red*) of the resonance will be beneficial for the (anti-)Stokes imaging.

Particles with a plasmon resonance slightly to the blue of the laser show an anti-Stokes emission roughly 10 times weaker than the Stokes emission. This would imply that the quantum yield of the emission at shorter wavelengths is 10 times smaller than the emission at longer wavelengths and therefore would be ~10^{-7} (13,20,32,33). The spectral dependence of the anti-Stokes emission, however, induces a large under estimation of the total intensity. The exponential shape seen in Fig. 1 implies that the majority of the emission is concentrated close to the laser excitation wavelength and therefore the filters are blocking it out. Careful experiments with narrower filters would allow a better characterization of the quantum yield of the anti-Stokes emission.
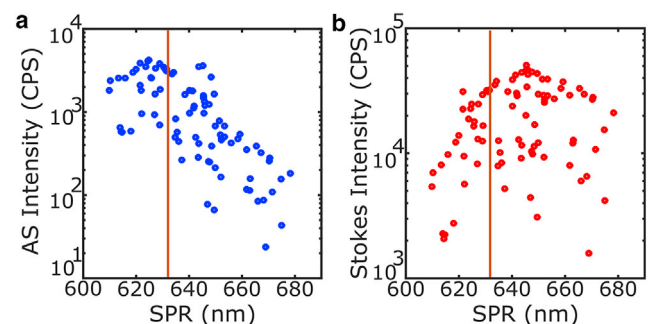

FIGURE 3 Emission intensity of different gold nanorods as a function of their plasmon peak position. The data are plotted for the anti-Stokes (*a*) and Stokes (*b*) sides of the emission; the orange vertical line at 633 nm is the wavelength of the laser. The anti-Stokes intensity was obtained by integrating the emission at wavelengths shorter than the laser, while the opposite was done for the Stokes. The spread in intensities for similar peak positions can be attributed to variations in sizes and, possibly, to different quantum yields of the different individual particles. The maximum emission for the anti-Stokes is obtained when the plasmon is slightly blue shifted from the excitation laser and vice versa for the Stokes emission. To see this figure in color, go online.

To prove that the technique is well suited for imaging particles in biological systems, we deposited HeLa cells on top of the nanorod sample.

Firstly, nanoparticles were deposited on clean glass coverslips by spin-casting a suspension of gold nanorods as described in Zijlstra and Orrit (31). This procedure ensures that the analysis is performed on single nanorods and therefore that the luminescence signals are not arising from clusters of nanorods. It also allowed us to characterize the nanorod emission both by acquiring spectra and by studying the dependency with excitation power, avoiding the diffusion away from the focus.

Secondly, HeLa cells were plated on top of these samples, and grown overnight until they reached a high confluency. Although the obtained images are not equivalent to images of gold nanorods residing in the cytoplasm or nucleus of cells, they would resemble very closely images of rods in cell membranes. This simplified protocol only serves the present purpose of optical signal/background characterization, and spared us the labor-intensive biocompatible particle functionalization that would be needed for more relevant biological assays. Fig. S5 shows a typical white light transmission image of the samples. The high confluency ensures that cells uniformly cover the entire observed area, so the studied nanorods are always localized below a cell. We have also acquired images of nanoparticles under cells containing the fluorescent dye Atto 647N. For this purpose the cells already attached to the coverslips were incubated with 45 pM Atto 647N for ~20 min. This set of experiments allowed us to compare Stokes and anti-Stokes emissions under high-background conditions.

RESULTS AND DISCUSSION

The nanoparticle shown in Fig. 1 displays comparable count rates for both the Stokes and anti-Stokes emissions. As explained earlier and shown in Fig. 3, this is because the excitation laser is slightly red shifted from the plasmon resonance, the most favorable position for enhancing the anti-Stokes part of the spectrum. Both types of emission are also comparable to the luminescence intensity obtained while exciting at 532 nm. The main difference is the laser intensity employed; the power density for exciting the transverse plasmon with the 532 nm laser was set to 80 kW/cm^2, while for both the anti-Stokes and Stokes, the 633 nm laser was set to 15 kW/cm^2, five times less intense. This suggests that the enhancement of absorption cross section at resonance more than compensates the loss of a significant fraction of the luminescence emission in the laser rejection filter, allowing us to use lower powers.

The three curves in Fig. 1 also show a very distinctive spectral distribution. The luminescence that arises from the 532 nm excitation spans almost 150 nm, from the laser wavelength up to >650 nm. The Lorentzian shape confirms that the emission arises from a single nanorod. The long-pass emission (*red curve*) spans a range of almost 100 nm, from the excitation at 633 nm to >700 nm. Finally, the anti-Stokes emission, which requires energy extraction from the thermal bath, cannot extend much beyond a few $k_B T$ from the excitation energy. This is the narrowest band, extending from the excitation to ~580 nm. The position of the plasmon resonance to the blue of the excitation laser explains the higher peak intensity of the anti-Stokes spectrum compared to the Stokes spectrum, whereas the total integrated Stokes emission is higher than the anti-Stokes's.

Fig. 4 shows two raster scans of the same $7.5 \times 7.5\ \mu m^2$ area of the sample with HeLa cells on top of gold nanorods. The left image shows the Stokes emission, where a 633 nm notch and 633 nm long-pass filter were employed. The right image corresponds to the anti-Stokes emission, where the same notch and a 633 nm short-pass filter were employed; in both cases the irradiation intensity was kept at 30 kW/cm^2 at the sample. Most particles are observed in both Stokes and anti-Stokes images but with different intensities. The main difference between the two images is the background count rate. The Stokes image has an average background count rate of ~5 kCPS, while the anti-Stokes is <100 CPS, close to 70 CPS, the dark counts of the detector. Moreover, in the Stokes image a structured background can be observed; we attribute this emission to self-fluorescence of the cells. On the other hand, the anti-Stokes image shows a much flatter background and highly distinguishable single particles. Both images display the count rate obtained after dark count subtraction.

The circled particles in Fig. 4 show the different possible situations: Particle 1 is the brightest both in Stokes and anti-Stokes, which can be explained if this is a bigger particle. Particles 2 and 3 are barely distinguishable in the Stokes image, while they are clearly visible in the anti-Stokes. This
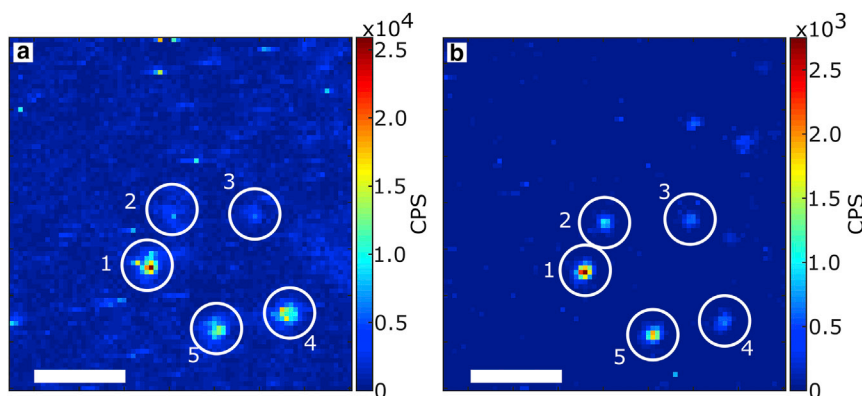

FIGURE 4 Raster scan of a nanorod sample under HeLa cells using (*a*) a long-pass filter and (*b*) a short-pass filter for photoluminescence detection. Some rods can be observed in both images, some others only in the Stokes or anti-Stokes images. Intensities in the Stokes and anti-Stokes emission thus do not necessarily correlate. The scale bar in both panels is 2 μm in length. To see this figure in color, go online.

can be attributed to a higher background level in the Stokes case and by a plasmon resonance of particles 2 and 3 to the blue of the laser, favoring the anti-Stokes emission process. Particles 4 and 5 are visible in both, but particle 4 is brighter than 5 in the Stokes image, while the opposite happens in the anti-Stokes. This is due to a plasmon position that favors more one or the other type of emission, as also shown in Fig. 3. Fig. S6 shows a larger area of the scan, where it is possible to observe more particles both in the Stokes and anti-Stokes configuration.

The use of the anti-Stokes emission is especially valuable when imaging nanoparticles in high background conditions. To this end we incubated the cells with a solution of Atto 647N. The fluorescent labeling of the cell, even if not specific, resulted in a similar situation to what would be obtained in the case of labeling organelles or the entire cell membrane. This dye was chosen because its absorption maximum is close to 633 nm, the excitation wavelength we employed in these experiments, but also because of its photostability and high quantum yield.

Fig. 5 shows two raster scans of the samples described above. The right panel shows the anti-Stokes image, in which single particles are clearly distinguishable and marked with a circle. We made sure that the observed spots were nanorods by monitoring their intensity under high illumination conditions and checking that they did not bleach. The left panel shows the Stokes emission, in which no particles can be distinguished from the background. The average background emission in the anti-Stokes image is <500 CPS, but higher than the dark counts of the detector. The Stokes emission, on the other hand, shows an average background intensity of ~200 kCPS that is one order of magnitude higher than that observed without the dye.

These results indicate that the Stokes image deteriorates much faster than the anti-Stokes in the presence of emitting molecules both from the cell itself or from added dyes. The images show regions with higher emission intensities in both configurations, most probably due to a higher concentration of dye in specific regions of the cell. Fig. S7 shows a larger scan, and the difference in background intensities is

more evident. At much higher concentrations than the ones shown in this work, the anti-Stokes emission from the dye becomes significant and can overcome the emission rate from individual particles.

Fig. 6 a shows the dependence of the acquired luminescence and the background as functions of excitation power for both the Stokes and anti-Stokes emissions of a particle below a cell without dye. Care was taken in choosing a particle with a resonance close to the excitation laser, to compare Stokes and anti-Stokes luminescence with similar resonant enhancements. The Stokes emission (*red curves*) shows a linear increase in signal together with a linear increase in background. In this case, the signal/background reaches a value of 6. The anti-Stokes emission (*blue curves*), however, shows a much steeper increase of the signal than the background, reaching a signal/background of 12. Of course, particles with a plasmon resonance to the blue of the laser wavelength show an even larger ratio of anti-Stokes to Stokes emission.

Fig. 6 b shows the same type of curves as Fig. 6 a, for a different particle under cells that contained Atto 647N. In this case the background prevented the acquisition of luminescence spectra; the particle chosen to draw the figure is representative of the average behavior. We see that in the Stokes case the particle's signal is barely larger than the fluorescence background from the dye. On the other hand, the anti-Stokes luminescence shows an enhanced contrast, reaching a signal/background >20 for this particular nanorod. The background level observed in the Stokes image increases much faster with dye content than the anti-Stokes background.

More particles under the same conditions were analyzed and their signal/background values are shown in Fig. S8. In this case, the irradiation intensity was kept at 30 kW/cm^2. The values of the ratio for Stokes and anti-Stokes under nonstained cells are similar and span roughly from 5 to 15. It is, however, important to note that on average the anti-Stokes emission is 10 times weaker than the Stokes one. It is remarkable that staining the cells with Atto 647N does not significantly alter the values obtained
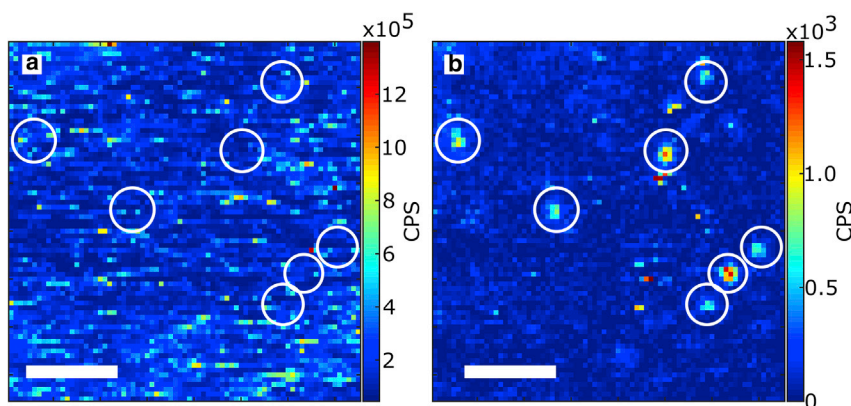

FIGURE 5 Raster scan of a nanorod sample covered by HeLa cells containing the fluorescent dye Atto 647N, again using (*a*) a long-pass filter and (*b*) a short-pass filter for photoluminescence detection. No clear nanorod signals can be seen in the Stokes images, whereas they are clearly distinguishable in the anti-Stokes image, proving the advantage of the latter for fluorescence background rejection. The scale bar in both panels is 2 μm in length. To see this figure in color, go online.

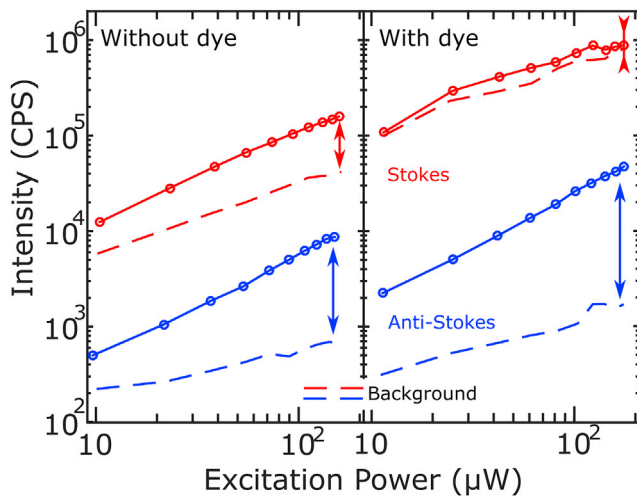FIGURE 6 Emission intensity (*solid lines*) and background (*broken lines*) as functions of excitation intensity for the Stokes (*red*) and the anti-Stokes (*blue*) emissions. These data were obtained on two different particles for the unstained cells (*right*) and stained cells (*left*). For the unstained cells, the plasmon was chosen close to the laser line, to avoid favoring one or the other emission by the resonance effect. (*Arrows*) Maximal signal/background of each emission in the figure conditions. To see this figure in color, go online.

for the anti-Stokes emission, while the Stokes emission was not separable from the background.

When the cells containing Atto 647N were used, we observed an increase in the background levels for both Stokes and anti-Stokes emission and these levels also depend on excitation power. This means that the dye shows both components, as is well known from fluorescence hot bands and anti-Stokes Raman scattering. The main difference between nanoparticles and dyes, however, is their quantum yield. While the particles appear to be relatively bright anti-Stokes emitters, in part due to their large absorption cross section, in part due to their plasmon resonance, dyes such as the one employed in this work, are much better Stokes emitters than anti-Stokes. This is the main reason why rods are drowned by the fluorescence background in the Stokes image.

The signal/background of the anti-Stokes emission increases with increasing laser excitation powers, going from values close to 2 for 3 kW/cm^2 excitation up to values of 20 for 53 kW/cm^2 as shown in Fig. 6 *b*. However, this cannot be extrapolated further than the results presented here. It is known that gold nanorods reshape under high irradiation intensities (34). For high-NA objectives like the one employed in this work, a rule of thumb to prevent reshaping in scanning confocal images is to keep the excitation intensity <150 μW at the back aperture of the objective lens (or equivalently a power density of 53 kW/cm^2 at the object plane).

In the presence of a fluorescent dye, the signal/background obtained is higher than in the case without dye.

This may be a consequence of the selection of particles with a plasmon more favorable to the anti-Stokes than to the Stokes emission, and could not be avoided by acquiring luminescence spectra because the background was too high. Although we checked the correct focusing on the sample plane both by optimizing the reflection on the glass/water interface and by employing the anti-Stokes signal, it was never possible to observe single particles under high background conditions in the Stokes configuration.

A major concern for the imaging of nanoparticles in cells is the local increase in temperature, widely exploited in plasmonic photothermal therapy (35). To calculate the raise in temperature induced by irradiating gold nanoparticles in resonance, we calculated the absorption cross section with the ADDA package (36). A particle with a length of 50 nm and diameter of 23 nm (the average dimensions of the ones employed in this work) has a maximum absorption cross section of 0.0117 μm^2. At an irradiation intensity of 20 kW/cm^2 and assuming all the absorbed energy is dissipated into heat gives a total power of 2.3 μW. This value is between 2 and 4 orders of magnitude lower than the reported threshold values for inducing cell death (37,38).

Moreover, we can estimate the temperature of the particle in the steady state by solving the Poisson equation. Assuming a spherical particle of the same volume as the average rod employed in this work and taking into account that the heat conductivity of the particle is much higher than that of the surrounding medium, it is possible to see that the increase in temperature on the surface of the particle follows

$$\Delta T(r) = \frac{Q_{abs}}{4\pi\kappa r},$$

where Q_{abs} is the absorbed power, κ is the heat conductivity of the medium, and r is the radius of the particle. By setting κ to 0.45 Wm^{-1} K^{-1} (39), we obtain a temperature increase on the surface of the particle of 25 K at an irradiation intensity of 20 kW/cm^2. Previous studies reported that the threshold temperature for inducing cell destruction is around a mean value of 74°C (37) or 50°C (40). In our case, the increase in temperature is concentrated locally around the nanoparticle; 50 nm away from the surface, the temperature increase of the medium is expected to be <5°C.

As a control, we also performed a viability test of the cells after the imaging process. We observed no difference between the cells that were on top of the imaged nanorods and those that were not, as shown in Fig. S9. The black square depicts the region that was imaged under the confocal microscope, while the rest was never irradiated with the laser. The white light transmission image also does not show any distinguishable changes before and after the imaging process. More rigorous tests of the particles inside cells are needed to confirm the harmlessness of the method.

CONCLUSION

In this work we have demonstrated that anti-Stokes photoluminescence arising from the excitation in (or close to) the plasmon resonance of a gold nanorod can be exploited to image them in biologically relevant conditions (25). The comparison between the Stokes and anti-Stokes emissions was possible by using particles immobilized on the substrate; however, the technique can be easily extended to imaging in fixed cells, in vivo or even for tracking particles in real time (6).

Extending this technique to wide-field should be possible considering the laser powers employed in this work. EMCCDs provide enough gain (41) to easily detect single nanoparticles, while at the same time the background is sufficiently low to give a high contrast. This extension of the technique would open the possibility to track at higher frame rates than achievable by confocal imaging.

The lower count rate of the anti-Stokes compared to the Stokes emission can be a drawback in such applications as localization (42). This technique's accuracy depends on the number of photons detected, and is given by $\approx 1/\sqrt{N}$, where N is the number of photons collected. The count rates obtained in this work are close to 1.5 kCPS, enough in many applications.

We have shown that the signal/background of the anti-Stokes emission is higher than that of the Stokes emission. In the case of HeLa cells not containing a fluorescent dye, typical values can be ~10 and 5, respectively, for a particle with a resonance at the laser wavelength. For HeLa cells containing Atto 647N, the difference is much more pronounced, because most of the particles will have a Stokes emission comparable or lower than the background, while in the anti-Stokes the signal/background can still be >10.

The main advantage of the technique presented in this work is that it can be easily implemented in any commercial or home-built microscope. It does not require a high investment in equipment or time, because filters are normally available for common laser wavelengths and there is no further need of modifying any experimental configuration already existent. Moreover, all the data analysis techniques employed in confocal or wide-field images for localization, tracking, etc., do not have to be modified.

SUPPORTING MATERIAL

Nine figures are available at http://www.biophysj.org/biophysj/supplemental/S0006-3495(16)30994-8.

AUTHOR CONTRIBUTIONS

A.C. performed the experiments, analyzed data, and wrote the article; V.I.P.K. prepared the samples and performed the experiments; M.J.M.S. designed the study; M.O. designed the study and wrote the article; and all authors analyzed the results and approved the final version of the article.

ACKNOWLEDGMENTS

REFERENCES

1. Moerner, W. E. 2007. New directions in single-molecule imaging and analysis. *Proc. Natl. Acad. Sci. USA.* 104:12596–12602.

2. Lichtman, J. W., and J.-A. Conchello. 2005. Fluorescence microscopy. *Nat. Methods.* 2:910–919.

3. Shaner, N. C., P. A. Steinbach, and R. Y. Tsien. 2005. A guide to choosing fluorescent proteins. *Nat. Methods.* 2:905–909.

4. Jana, N. R., L. Gearheart, and C. J. Murphy. 2001. Wet chemical synthesis of high aspect ratio cylindrical gold nanorods. *J. Phys. Chem. B.* 105:4065–4067.

5. Alkilany, A. M., L. B. Thompson, …, C. J. Murphy. 2012. Gold nanorods: their potential for photothermal therapeutics and drug delivery, tempered by the complexity of their biological interactions. *Adv. Drug Deliv. Rev.* 64:190–199.

6. van den Broek, B., B. Ashcroft, …, J. van Noort. 2013. Parallel nanometric 3D tracking of intracellular gold nanorods using multifocal two-photon microscopy. *Nano Lett.* 13:980–986.

7. Pérez-Juste, J., I. Pastoriza-Santos, …, P. Mulvaney. 2005. Gold nanorods: synthesis, characterization and applications. *Coord. Chem. Rev.* 249:1870–1901.

8. Mohamed, M. B., V. Volkov, …, M. A. El-Sayed. 2000. The 'lightning' gold nanorods: fluorescence enhancement of over a million compared to the gold metal. *Chem. Phys. Lett.* 317:517–523.

9. Yao, S., H. H. Cai, …, P. H. Yang. 2014. Fluorescent labeling of cellular targets and multicolor imaging with gold nanorods. *Dyes Pigments.* 101:286–294.

10. Spillane, K. M., J. Ortega-Arroyo, …, P. Kukura. 2014. High-speed single-particle tracking of GM1 in model membranes reveals anomalous diffusion due to interleaflet coupling and molecular pinning. *Nano Lett.* 14:5390–5397.

11. Urban, A. S., T. Pfeiffer, …, J. Feldmann. 2011. Single-step injection of gold nanoparticles through phospholipid membranes. *ACS Nano.* 5:3585–3590.

12. Lewinski, N., V. Colvin, and R. Drezek. 2008. Cytotoxicity of nanoparticles. *Small.* 4:26–49.

13. Yorulmaz, M., S. Khatua, …, M. Orrit. 2012. Luminescence quantum yield of single gold nanorods. *Nano Lett.* 12:4385–4391.

14. Link, S., M. B. Mohamed, and M. A. El-Sayed. 1999. Simulation of the optical absorption spectra of gold nanorods as a function of their aspect ratio and the effect of the medium dielectric constant. *J. Phys. Chem. B.* 103:3073–3077.

15. Berciaud, S., D. Lasne, …, B. Lounis. 2006. Photothermal heterodyne imaging of individual metallic nanoparticles: theory versus experiment. *Phys. Rev. B.* 73:045424.

16. Ignatovich, F. V., and L. Novotny. 2006. Real-time and background-free detection of nanoscale particles. *Phys. Rev. Lett.* 96:013901.

17. Bouhelier, A., R. Bachelot, …, G. P. Wiederrecht. 2005. Surface plasmon characteristics of tunable photoluminescence in single gold nanorods. *Phys. Rev. Lett.* 95:267405.

18. Dulkeith, E., T. Niedereichholz, …, F. Caruso. 2004. Plasmon emission in photoexcited gold nanoparticles. *Phys. Rev. B.* 70:205424.

19. Link, S., and M. A. El-Sayed. 2000. Shape and size dependence of radiative, non-radiative and photothermal properties of gold nanocrystals. *Int. Rev. Phys. Chem.* 19:409–453.

20. Rao, W., Q. Li, …, L. Wu. 2015. Comparison of photoluminescence quantum yield of single gold nanobipyramids and gold nanorods. *ACS Nano.* 9:2783–2791.

21. Ngoc, Ll. T., J. Wiedemair, …, E. T. Carlen. 2015. Plasmon-modulated photoluminescence from gold nanostructures and its dependence on plasmon resonance, excitation energy, and band structure. *Opt. Express.* 23:5547–5564.

22. Nikoobakht, B., and M. A. El-Sayed. 2003. Preparation and growth mechanism of gold nanorods (NRs) using seed-mediated growth method. *Chem. Mater.* 15:1957–1962.

23. Ni, W., X. Kou, …, J. Wang. 2008. Tailoring longitudinal surface plasmon wavelengths, scattering and absorption cross sections of gold nanorods. *ACS Nano.* 2:677–686.

24. He, Y., K. Xia, …, Q. Gong. 2015. Surface enhanced anti-Stokes one-photon luminescence from single gold nanorods. *Nanoscale.* 7:577–582.

25. Jiang, L., I. W. Schie, …, T. Huser. 2013. Coherent anti-Stokes emission from gold nanorods and its potential for imaging applications. *ChemPhysChem.* 14:1951–1955.

26. Sönnichsen, C., T. Franzl, …, P. Mulvaney. 2002. Drastic reduction of plasmon damping in gold nanorods. *Phys. Rev. Lett.* 88:077402.

27. Lin, Z., L. V. Zhigilei, and V. Celli. 2008. Electron-phonon coupling and electron heat capacity of metals under conditions of strong electron-phonon nonequilibrium. *Phys. Rev. B.* 77:1–17.

28. Sun, C., F. Vallée, …, J. G. Fujimoto. 1994. Femtosecond-tunable measurement of electron thermalization in gold. *Phys. Rev. B Condens. Matter.* 50:15337–15348.

29. Huang, J., W. Wang, …, D. G. Cahill. 2014. Resonant secondary light emission from plasmonic Au nanostructures at high electron temperatures created by pulsed-laser excitation. *Proc. Natl. Acad. Sci. USA.* 111:906–911.

30. Neupane, B., L. Zhao, and G. Wang. 2013. Up-conversion luminescence of gold nanospheres when excited at nonsurface plasmon resonance wavelength by a continuous wave laser. *Nano Lett.* 13:4087–4092.

31. Zijlstra, P., and M. Orrit. 2011. Single metal nanoparticles: optical detection, spectroscopy and applications. *Rep. Prog. Phys.* 74:106401.

32. Cheng, Y., G. Lu, …, Q. Gong. 2016. Luminescence quantum yields of gold nanoparticles varying with excitation wavelength. *Nanoscale.* 8:2188–2194.

33. Fang, Y., W.-S. Chang, …, S. Link. 2012. Plasmon emission quantum yield of single gold nanorods as a function of aspect ratio. *ACS Nano.* 6:7177–7184.

34. Liu, Y., E. N. Mills, and R. J. Composto. 2009. Tuning optical properties of gold nanorods in polymer films through thermal reshaping. *J. Mater. Chem.* 19:2704.

35. Huang, X., P. K. Jain, …, M. A. El-Sayed. 2008. Plasmonic photothermal therapy (PPTT) using gold nanoparticles. *Lasers Med. Sci.* 23:217–228.

36. Yurkin, M. A., and A. G. Hoekstra. 2011. The discrete-dipole-approximation code ADDA: capabilities and known limitations. *J. Quant. Spectrosc. Radiat. Transf.* 112:2234–2247.

37. Huang, X., P. K. Jain, …, M. A. El-Sayed. 2006. Determination of the minimum temperature required for selective photothermal destruction of cancer cells with the use of immunotargeted gold nanoparticles. *Photochem. Photobiol.* 82:412–417.

38. Huang, X., I. H. El-Sayed, …, M. A. El-Sayed. 2006. Cancer cell imaging and photothermal therapy in the near-infrared region by using gold nanorods. *J. Am. Chem. Soc.* 128:2115–2120.

39. Sturesson, C., and S. Andersson-Engels. 1995. A mathematical model for predicting the temperature distribution in laser-induced hyperthermia. Experimental evaluation and applications. *Phys. Med. Biol.* 40:2037–2052.

40. O'Neal, D. P., L. R. Hirsch, …, J. L. West. 2004. Photo-thermal tumor ablation in mice using near infrared-absorbing nanoparticles. *Cancer Lett.* 209:171–176.

41. Dussault, D., and P. Hoess. 2004. Noise performance comparison of ICCD with CCD and EMCCD cameras. *Opt. Sci. Technol. SPIE 49th Annu. Meet.* 195–204.

42. Sahl, S. J., and W. E. Moerner. 2013. Super-resolution fluorescence imaging with single molecules. *Curr. Opin. Struct. Biol.* 23:778–787.

Supplemental Information

Background Suppression in Imaging Gold Nanorods through Detection of Anti-Stokes Emission

Aquiles Carattino, Veer I.P. Keizer, Marcel J.M. Schaaf, and Michel Orrit

Background suppression in imaging gold nanorods through detection of anti-Stokes emission

A. Carattino, V.I.P. Keizer, M.J.M Schaaf, and M. Orrit

E-mail:

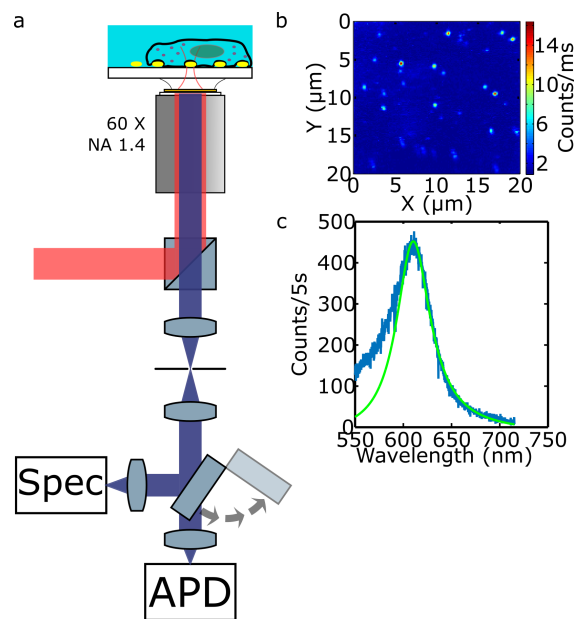## Setup

Figure S1: Experimental setup and examples of observations. a) Simplified schematic of the confocal microscope employed during the measurements. b) A typical 1-photon luminescence raster scan of the sample immersed in water c) luminescence spectrum of a single rod.

Figure S1 shows the schematic of the confocal microscope employed in the experiments. It is important to note the presence of a 50/50 beamsplitter before the objective. Exchanging

1

it for an appropriate dichroic mirror would increase the collection efficiency. In this work we chose not to do it because the beamsplitter allows to collect both the full emission under 532 nm excitation and the Stokes/anti-Stokes emission under 633 nm without changes in the optical path.
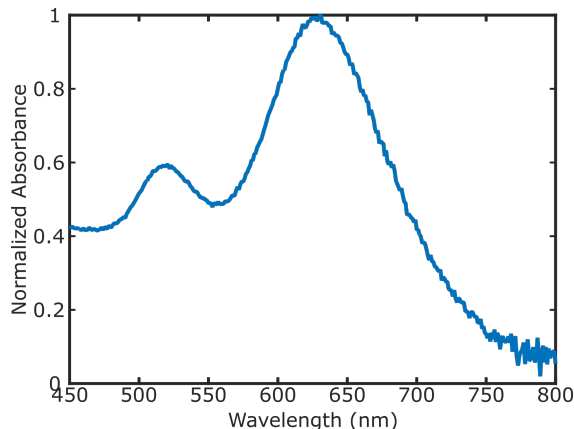
Uv-Vis spectrum

Figure S2: Normalized extinction spectrum of a suspension of nanorods after synthesis. The resonance maximum is located at 630 nm.

Figure S2 shows the extinction spectrum of the nanorod samples used throughout this work. Two peaks are clearly distinguishable, one around 630 nm that corresponds to the longitudinal plasmon resonance (LPR) of particles with sizes 50 nm × 23 nm and a second one at around 520 nm. This peak also includes contributions of spheres as by-products of the synthesis of the rods. The transverse plasmon resonance is also located at the same wavelength but is much weaker than the LPR. In a sample consisting exclusively of rods, the transverse resonance would be barely observable in a UV-Vis spectrometer.

Filters

The selection of filters plays a crucial role in the signal acquired. Since the main part of the anti-Stokes emission is concentrated around the excitation wavelength, it is important
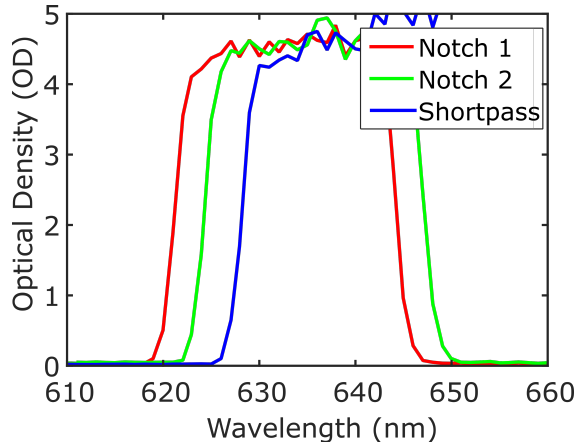
Figure S3: Transmission spectrum of two notch filters and a short pass filter (Semrock).

to select filters that have a high transmission close to the laser line. Figure S3 shows the normalized absorption spectrum of two notch filters and a short pass. Both notch filters are branded as $NF03 - 633E - 25$ but show a slightly different absorption spectrum, shifted roughly $4\,nm$ from each other. The shortpass filter (branded as $SP01 - 633RU - 25$) shows the transition to transmission even closer to the laser line.

For many fluorescence applications the exact shape of the transmission spectrum of the filters does not play a crucial role. However for anti-Stokes imaging, since the shape of the emission is exponential-like, minute changes in the transmission spectrum can have a great impact on the signal collected. For example, changing from a detection path with a spectrum like notch 1 to one like shortpass (i.e. shifting in about $7\,nm$ the edge of the filter) increases the collected number of photons by about 50%.

In this work, since only one filter does not provide enough attenuation, care was taken to always employ the notch with the most favorable transmission spectrum in combination with either a shortpass or a longpass filter. Ideally, two shortpass filters would have been the best solution.
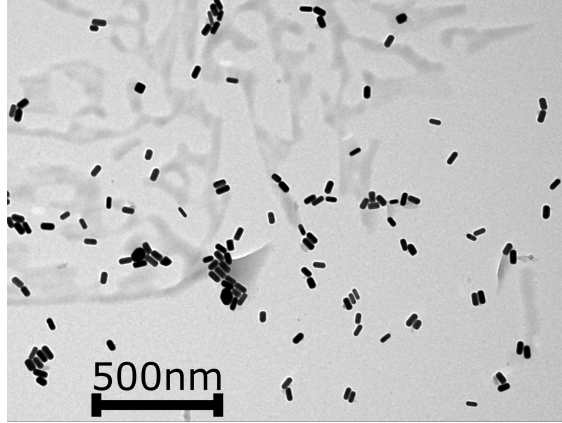
Figure S4: TEM image of the nanorod sample. The scale bar is $500\,\mu$m.

TEM Images of rods

Figure S4 shows an example TEM image of the gold nanorod sample. Analysis on the dimensions of the particles yield an average length of $50\,$nm and diameter of $23\,$nm. This is consistent with the plasmon observed in fig. S2 and at a single-particle level as in fig. S1c.

White light transmission

Full scan without dye

The raster scan shown in Figure S6 corresponds to a larger area comprising the same region shown in the main text. The majority of the particles has a much larger contrast in the anti-Stokes. Moreover it can be noted that the background is flat. In the Stokes image the nanorods are still visible, but the contrast is obviously lower.

Full scan without dye

Figure S7 shows a raster scan of gold nanorods under cells stained with Atto 647N. Both images comprise the same region shown in the main text, here marked with a black square. No particles can be detected in the Stokes image, while several nanorods are visible in the
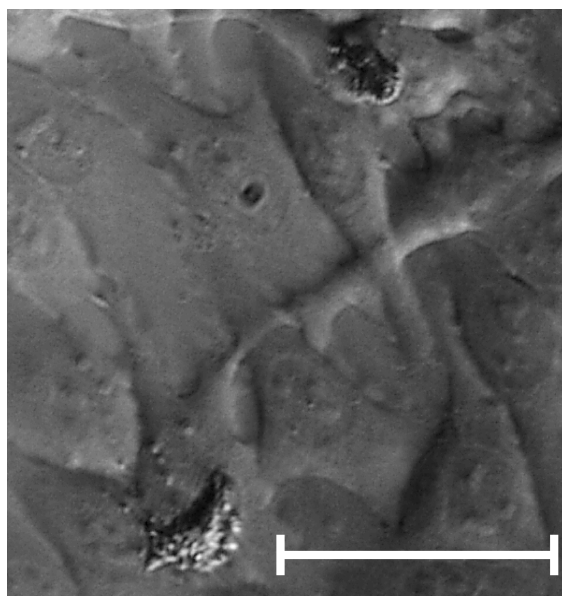
Figure S5: White light transmission image of the sample with cells deposited on top of the rods. It is possible to observe that they cover entirely the observed region without spacing in between them. The scale bar in the figure is $20\,\mu$m in length.
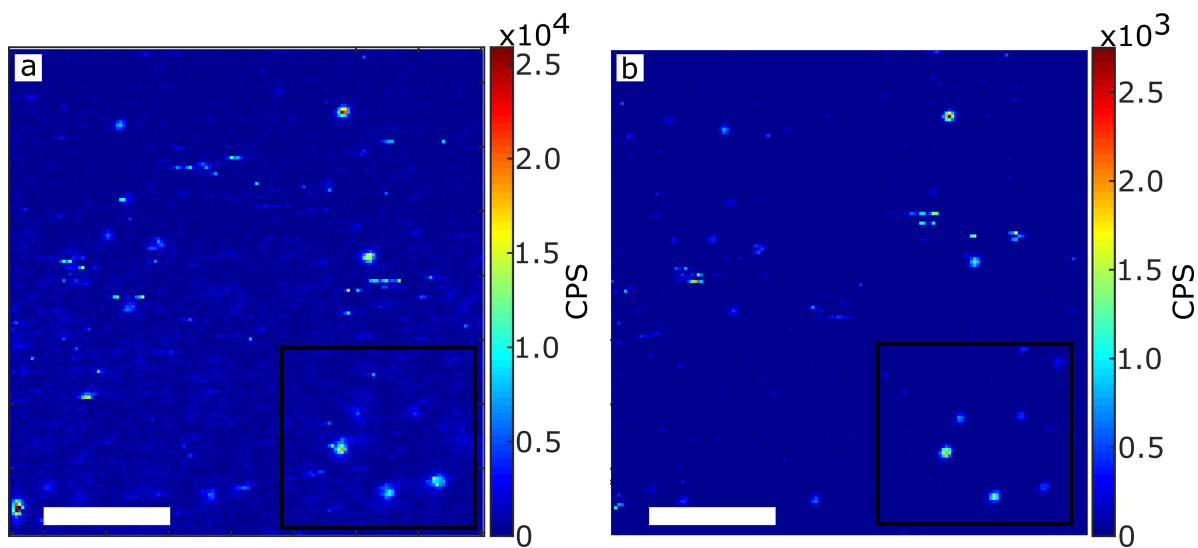

Figure S6: Raster scan of a nanorod sample under HeLa cells using (a) a long pass filter and (b) a short pass filter for photoluminescence detection. Both scans contain the same region shown in the main text and here marked with a black square. The scale bar in both figures is $4\,\mu$m in length.
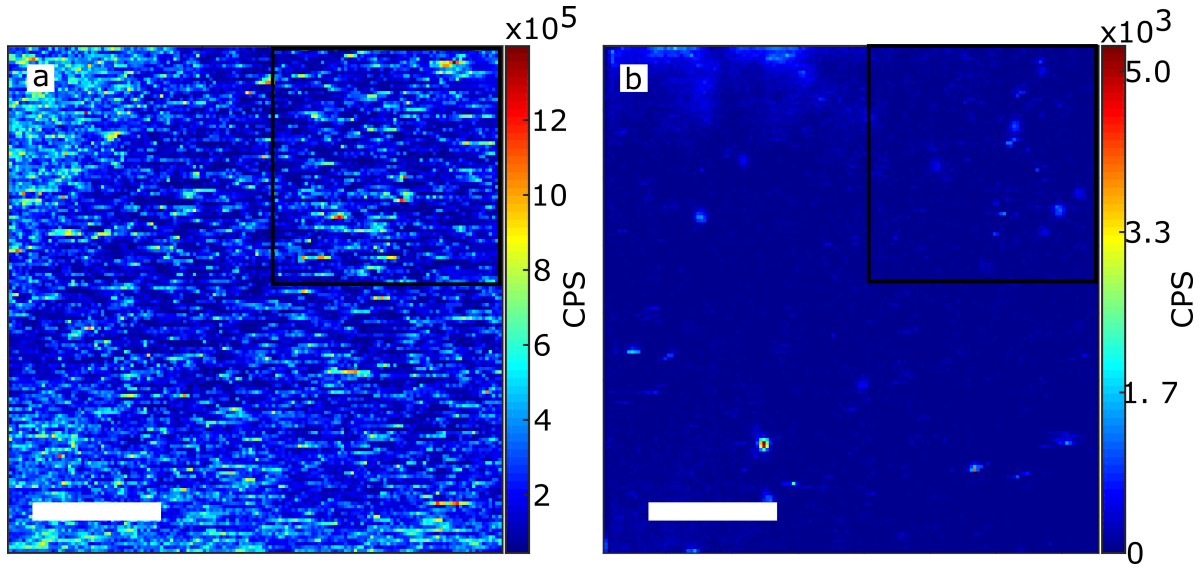
Figure S7: Raster scan of a nanorod sample under stained HeLa cells using (a) a long pass filter and (b) a short pass filter for photoluminescence detection. Both scans contain the same region shown in the main text and here marked with a black square. The scale bar in both figures is $4\,\mu$m in length.

anti-Stokes image with a high signal-to-background. We note, however, that there is some background appearing in the top left part of the anti-Stokes image. This may be due to an increase of the concentration of Atto 647N. The incubation procedure does not prevent the accumulation of dye in specific organelles of the cells, and there is no control on the final dye concentration.

Signal-to-background of several particles

Figure S8 shows the distribution of signal-to-background ratios for several particles. The data were acquired with an irradiation intensity of $30\,\mathrm{kW/cm^2}$. Fig. S8a shows the distribution for nanoparticles under unstained cells. It is possible to observe a broad distribution of values between ratios of 5 and 15. Fig. S8b shows the signal-to-background distribution for the anti-Stokes emission, concentrated mainly between 5 and 10. Finally Figure S8c shows the anti-Stokes signal-to-background ratio of particles under cells stained with Atto 647N. In this case it is possible to observe a similar distribution of values. Stokes data under stained
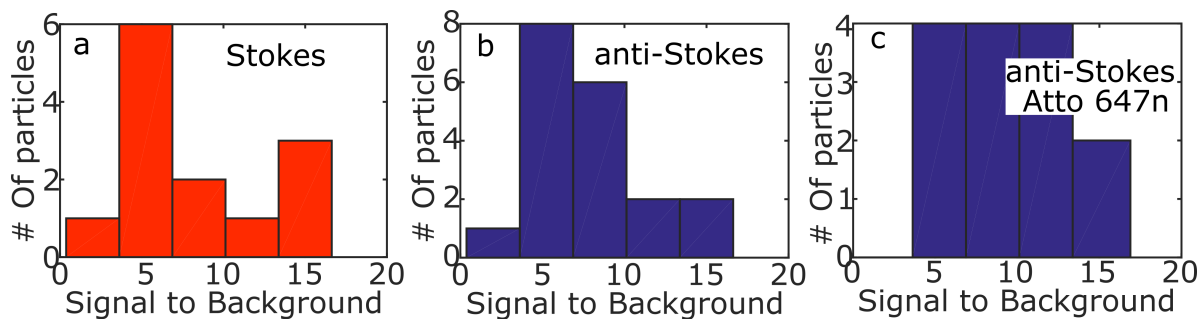
Figure S8: Histograms of the signal-to-background of several particles irradiated at $30\,\mathrm{kW/cm^2}$. a) Stokes emission under unstained cells, b) same but anti-Stokes emission, c) anti-Stokes under cells stained with Atto 647N.

cells are not presented because it was impossible to detect single nanoparticles under those conditions.
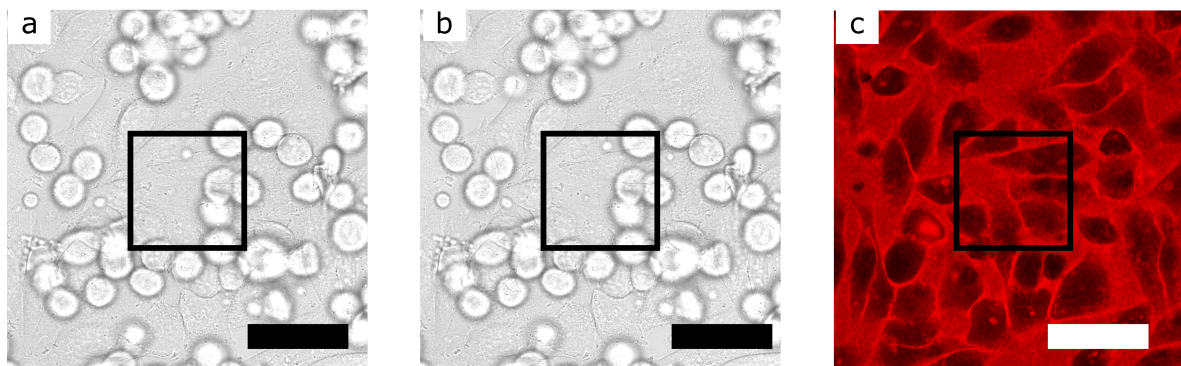
Viability test

Figure S9: White light transmission image of the cells, a) before being irradiated with the 633 nm laser, b) after the imaging process and c) viability test. The black square represents the imaged area. The scale bar is $50\,\mu$m.

To support the claim of the harmlessness of the method proposed in this work, we performed a standard viability test of the cells after imaging. Figure S9 shows white light transmission images of the cells. The left figure is before the imaging of the nanorods, the central is after and the rightmost is the result of a viability test with trypan blue. The black square represents the area that was imaged with the confocal microscope. The cells show no change between before and after the procedure. Moreover in Fig. S9c it is possible to see

7

that the dye did not enter the cells, therefore their membrane was intact after the imaging process.

More rigorous tests of viability after imaging the nanorods inside the cells are needed, but they are outside the scope of this work. On one hand there is enough evidence showing that gold nanoparticles are not toxic for cells.[1,2] On the other hand two photon imaging[3] or photothermal heterodyne detection[4] of particles inside cells did not destroy them. Continuous wave confocal imaging as presented here however was not studied in detail in the past mainly because of the poor signal-to-background ratio with the normal Stokes configuration.

References

(1) Huff, T. B.; Hansen, M. N.; Zhao, Y.; Cheng, J.-x.; Wei, A. Controlling the Cellular Uptake of Gold Nanorods. *Langmuir* **2007**, *23*, 1596–1599.

(2) Lewinski, N.; Colvin, V.; Drezek, R. Cytotoxicity of nanopartides. *Small* **2008**, *4*, 26–49.

(3) van den Broek, B.; Ashcroft, B.; Oosterkamp, T. H.; van Noort, J. Parallel Nanometric 3D Tracking of Intracellular Gold Nanorods Using Multifocal Two-Photon Microscopy. *Nano Lett.* **2013**, *13*, 980–986.

(4) Leduc, C.; Si, S.; Gautier, J.; Soto-Ribeiro, M.; Wehrle-Haller, B.; Gautreau, A.; Giannone, G.; Cognet, L.; Lounis, B. A highly specific gold nanoprobe for live-cell single-molecule imaging. *Nano Lett.* **2013**, *13*, 1489–94.